




Synthesis of Cu–CdIn₂O₄ nanoparticles decorated on nickel foam as a sensitive non-enzymatic electrochemical sensor for glucose detection

Xu Tian¹, Sijia Peng¹, Hui Shu¹, Tingrun Lai¹, Zhichao Yang¹, Ting Chen^{2,*}, Xuechun Xiao^{3,*}, and Yude Wang^{1,*} 

¹School of Materials and Energy, Yunnan University, Kunming 650091, People's Republic of China

²Institute of Materials Science & Devices, School of Materials Science and Engineering, Suzhou University of Science and Technology, Suzhou 215009, People's Republic of China

³Yunnan Key Laboratory of Carbon Neutrality and Green Low-Carbon Technologies, Yunnan University, Kunming 650091, People's Republic of China

Received: 26 April 2022

Accepted: 25 June 2022

Published online:

23 July 2022

© The Author(s), under exclusive licence to Springer Science+Business Media, LLC, part of Springer Nature 2022

ABSTRACT

Fast and effective detection of glucose has important significance in clinical medicine and the diagnosis of diabetes. Electrochemical non-enzymatic glucose sensor has received extensive attention to detect glucose in the recent years due to its simple operation and low cost. In this paper, Cu–CdIn₂O₄ nanoparticles decorated on nickel foam electrode as a sensitive non-enzymatic electrochemical sensor for glucose detection are synthesized by a one-step non-aqueous sol–gel method. Different Cu-doping levels are designed as performance comparison analysis. The electrocatalytic performance of the Cu–CdIn₂O₄ nanoparticles/Ni foam electrodes towards glucose oxidation is evaluated by cyclic voltammetry and current time. The results show that 15% Cu–CdIn₂O₄/Ni foam electrode shows higher sensitivity, as well as an excellent anti-interference and long-term stability towards glucose detection compared with 10% and 20% Cu–CdIn₂O₄/Ni foam electrodes. Hence, 15% Cu–CdIn₂O₄/Ni foam can be regarded as an efficient and a promising sensing material for glucose detection. Such satisfactory performance is not only attributed to the synergistic effect of Cd, In, and Cu, but also benefits from the uniform distribution of 15% Cu–CdIn₂O₄ nanoparticles on the Ni foam, which provides more reactive sites for the electrochemical catalytic reaction.

Address correspondence to E-mail: chenting@mail.usts.edu.cn; xchxiao@ynu.edu.cn; ydawang@ynu.edu.cn

1 Introduction

Glucose is an energy source and an intermediate product of metabolism for living cells in the human body. Glucose is easily absorbed into the blood to maintain the body's functional activities, but once the levels are above 7 mmol/L it can lead to diabetes. Diabetes is a serious metabolic disease that poses a great threat to human health and produces a series of complications. Therefore, it is of great significance to use an appropriate way to real-time monitor glucose level for human health protection and disease prevention. Currently, various methods such as fluorescent [1], optical [2], acoustic [3], and electrochemical methods [4] have been widely used to detect glucose, among which electrochemical glucose sensors [5, 6] including enzymatic glucose sensor and non-enzymatic glucose sensor [7] have received extensive interest and achieved great success due to their ease of operation, stable, fast, accurate, and reliable test results [8, 9]. Enzymatic glucose sensors usually use glucose oxidase (GOx) or glucose dehydrogenase (GDH) as biological catalysts to accelerate the oxidation of glucose, so as to achieve the purpose of detection. Although the enzymatic glucose sensor has exhibited some merits such as high sensitivity and good selectivity, its application is limited to a certain extent due to high price, easy to be affected by the surrounding environment, and poor long-term stability. To tackle the issues, more efforts have been devoted on the development of non-enzymatic glucose sensor with low cost, ease of operation, high sensitivity, and good stability. Different from the enzymatic glucose sensors, the non-enzymatic glucose sensors use inorganic materials as catalysts to realize the oxidation of glucose in neutral and alkaline environment. To date, various nanomaterials such as noble metals [10], metal nitrides [11–13], metal oxides [14–16], metal sulfides [17–20], metal alloys [21, 22], and metal hydrate [23] have been extensively developed for non-enzymatic glucose sensors. Among them, metal oxides based non-enzymatic glucose sensors are the most widely studied due to their low cost, excellent electrocatalytic activities, and superior stability [24]. Especially, the bimetallic oxides with the structure AB_2O_4 such as $MnCo_2O_4$ [25], $CuGa_2O_4$ [26], $NiCo_2O_4$ [27] $CuCo_2O_4$ [28], and $NiGa_2O_4$ [29] have been considered as promising catalysts for glucose oxidation due to the synergistic effect of bimetals.

$CdIn_2O_4$ is a typical n-type bimetallic oxide [30] with metal-like high conductivity, bimetallic synergy, and excellent electrical properties, which can be used as a ideal catalyst for glucose oxidation. To the best of our knowledge, $CdIn_2O_4$ nanomaterials have been rarely reported for electrochemical analysis. More importantly, numerous reports have indicated that composite materials exhibit obvious advantages in improving performance by using their synergistic effects compared with the single component materials. At present, there are only few reports on elements doped by $CdIn_2O_4$, appropriate doping has been considered an effective method to enhance the electrochemical properties by providing electronic defects and changing the electrical conductivity. Transition metals such as Cr, Cu, Ni, Co, and Fe often act as appropriate dopants in various fields since they change the original crystal parameters and enhance the catalytic activity [31].

In this work, Cu-doped $CdIn_2O_4$ nanoparticles decorated on Ni foam are synthesized by a one-step non-aqueous sol-gel method. This novel Cu-doped $CdIn_2O_4$ nanoparticles/Ni foam electrodes can be used as a non-enzymatic sensor for electrocatalytic oxidation of glucose. Several characterization techniques and electrochemical instruments are applied to evaluate the properties of the nanomaterials. As expected, the obtained Cu-doped $CdIn_2O_4$ nanoparticles/Ni foam electrodes display excellent electrocatalytic properties, high sensitivity, and fast response time for glucose detection.

2 Experimental

2.1 Material and reagents

Indium nitrate hydrate ($InN_3O_9 \cdot xH_2O$, 99.9%), Cadmium acetate ($Cd(CH_3CO_2)_2$, 99.5%), benzyl alcohol (C_7H_8O , 99.8%), and cupric acetate ($C_4H_6CuO_4 \cdot H_2O$, 99.0%) are purchased from Macklin Biochemical Co., Ltd (Shanghai, China). Nickel foam (Ni foam) is supplied by Lizhiyuan Battery Materials Co., Ltd (Shanxi, China). All chemical reagents are analytical grade in this experiment and without any further purification.

2.2 Synthesis of Cu–CdIn₂O₄ nanoparticles decorated on Ni foam

Firstly, Ni foams (1 cm × 2 cm) are cut and immersed in dilute hydrochloric acid solution for 12 h to remove impurities, and then are washed with DI water and absolute ethyl alcohol alternately. Subsequently, the treated Ni foams are dried at 60 °C for further use. The pure CdIn₂O₄ nanoparticles decorated on Ni foam are synthesized according to our previous report [32]. The Cu–CdIn₂O₄ nanoparticles decorated on Ni foam are synthesized by a one-step non-aqueous sol–gel method. The schematic illustrations of the synthesis and electrochemical glucose detection process of the Cu–CdIn₂O₄ nanoparticles electrode are shown in Fig. 1. Typically, 0.4512 g InN₃O₉·xH₂O and 0.3999 g Cd(CH₃CO₂)₂ are added to 60 mL C₇H₈O solvent. Then, a certain amount of C₄H₆CuO₄·H₂O with different mass ratio to pure CdIn₂O₄ nanoparticles (10, 15, and 20%) and the treated Ni foams are added into the above solution, followed by stirring for 12 h to get the homogeneous solution. Then the obtained solution is transferred to 100 mL Teflon-lined stainless steel autoclave and maintained at 200 °C for 48 h. After the reaction is over, the autoclave is cooled to room temperature naturally, the decorated Ni foams and

resulting precipitates are washed several times by centrifugation with ethanol and DI water alternately and dried at 60 °C in air for further investigation.

2.3 Characterization

X-ray diffraction (XRD; D/Max-3B, Rigaku, Japan) with CuKα1 radiation ($\lambda = 0.15406$ nm, 40 kV, 100 mA) is applied to analyze the crystal phase of the samples. Scanning electron microscopy (SEM, Quanta 200, FEI, America) and transmission electron microscopy (TEM, JEM-2010, JEOL, Japan) are conducted to investigate the morphology of the samples. X-ray photoelectron spectroscopy (XPS, ESCALAB 250, Thermo Fisher Scientific, America) and energy-dispersive spectroscopy (EDS; Bruker Nano GMBH, Germany) are applied to determine the chemical states and the chemical compositions. The samples characterized by XRD, TEM, EDS, and XPS are powder samples shaken by ultrasonic method on Ni foam.

2.4 Electrochemical measurements

The electrochemical measurements are performed on the CHI 760 electrochemical workstation (CH Instruments Co., Shanghai, China). A conventional

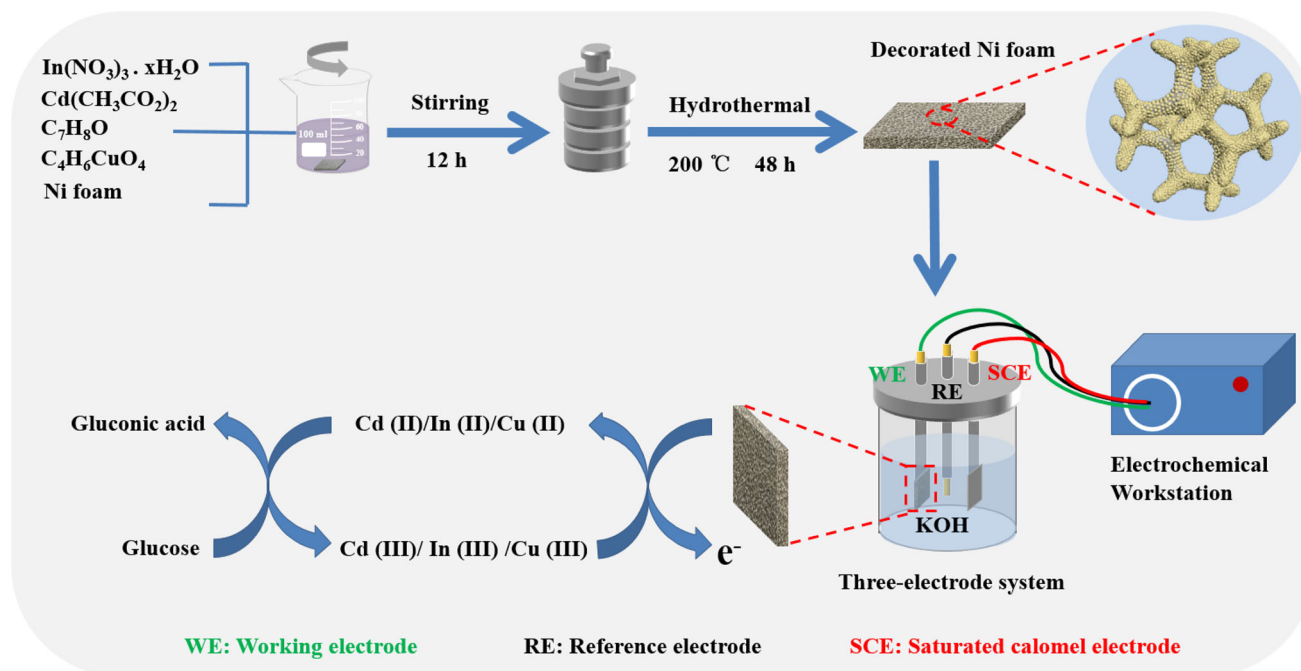


Fig. 1 The schematic illustrations of the synthesis and electrochemical glucose detection process of the Cu–CdIn₂O₄ nanoparticles/Ni foam electrodes

three-electrode system is employed, including the decorated Ni foams with Cu–CdIn₂O₄ nanoparticles as the working electrode, a platinum sheet as the counter electrode, and a saturated calomel electrode (SCE) as the reference electrode. Electrochemical analysis is performed in a 200 mL 3.5 M KOH electrolyte solution at room temperature, including the current time (*I*–*t*), cyclic voltammetry (CV) and electrochemical impedance spectroscopy (EIS). The *I*–*t* curve represents the current changes caused by glucose redox reaction at a constant voltage of 0.45 V. CV curve is characterized in the potential range of -0.075 V to 0.675 V at a scan rate of 50 mV s⁻¹. EIS is carried out at the equilibrium potential of open circuit, and the frequency range is selected as 0.01–10⁵ Hz in 3.5 M KOH electrolyte solution.

3 Results and discussions

3.1 Characterization

The XRD patterns of pristine CdIn₂O₄, 10%, 15%, and 20% Cu-doped CdIn₂O₄ samples are shown in Fig. 2a. All diffraction peaks of the un-doped, 10%, and 15% Cu-doped CdIn₂O₄ are well attributed to the phase of CdIn₂O₄, and there are no other byproducts detected, which imply that the Cu ions incorporate into the lattice of CdIn₂O₄ without destroying the crystal structure. While for 20% Cu-doped CdIn₂O₄, in addition to the phase with CdIn₂O₄, the phase of Cd(OH)₂ is also clearly observed, indicating that

when the content of Cu is too high, more Cd ions in CdIn₂O₄ would be replaced by Cu ions, since the Cd and Cu ions have small difference in ionic radius, 0.095 and 0.073 nm, respectively. The displaced Cd ions react with hydroxy (–OH) in benzyl alcohol to generate Cd(OH)₂. Furthermore, the doping of Cu changes the lattice constants of CdIn₂O₄. Typically, from the enlarged diffraction peak of (311) plane shown in Fig. 2b, it is understood that the position of the diffraction peak has a slight shift to a large angle with Cu doping, indicating that Cu ions incorporate into the lattice of CdIn₂O₄ and cause the lattice to shrink, and the interplanar spacing to decrease (according to Bragg's law, the interplanar spacing is inversely proportional to the diffraction angle).

Figure 3 systematically performs the morphological features of the obtained Cu–CdIn₂O₄ nanoparticles decorated on Ni foams. The SEM images of 10%, 15%, and 20% Cu–CdIn₂O₄ nanoparticles decorated on Ni foams are shown in Fig. 3a, b, and c, respectively. One can observe that there are obvious differences in the morphology of the as-prepared products with the content of Cu doping. Among them, 10% and 20% Cu–CdIn₂O₄ products take on a coral-flower appearance composed of several thin short sticks. For 15% Cu–CdIn₂O₄, multiple irregular clusters resembling ice flowers particles are observed, meanwhile, the smaller morphology size of 15% Cu–CdIn₂O₄ possesses higher specific surface area and reactive sites compared with 10% and 20% Cu–CdIn₂O₄, which helps to improve the electrochemical performance and glucose detection. Figure 3d

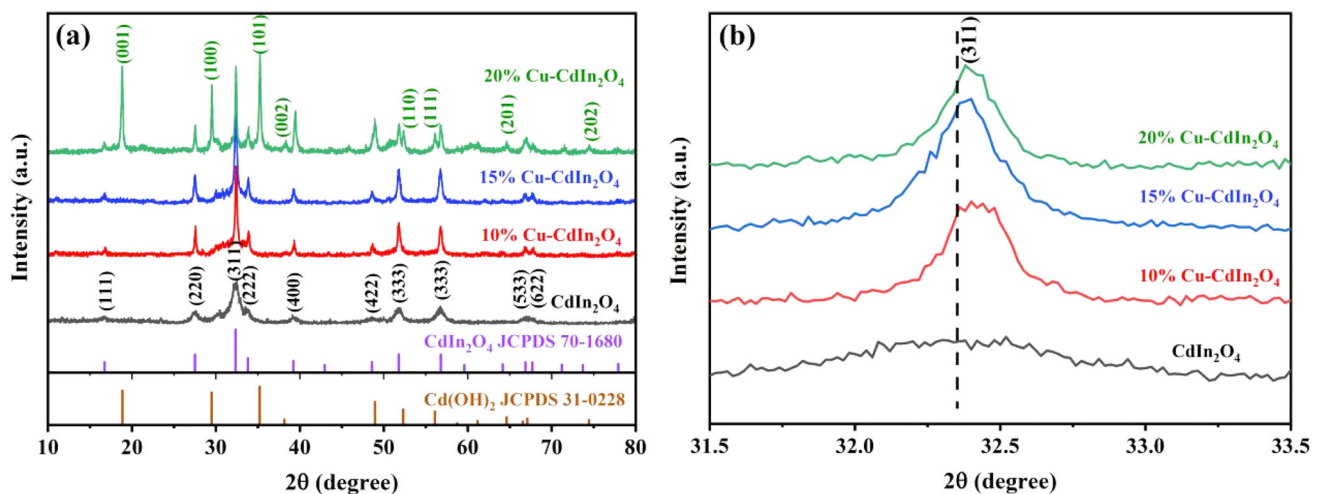


Fig. 2 The X-ray diffraction patterns: **a** CdIn₂O₄, 10% Cu–CdIn₂O₄, 15% Cu–CdIn₂O₄, and 20% Cu–CdIn₂O₄. **b** Enlarged diffraction peak of (311) plane

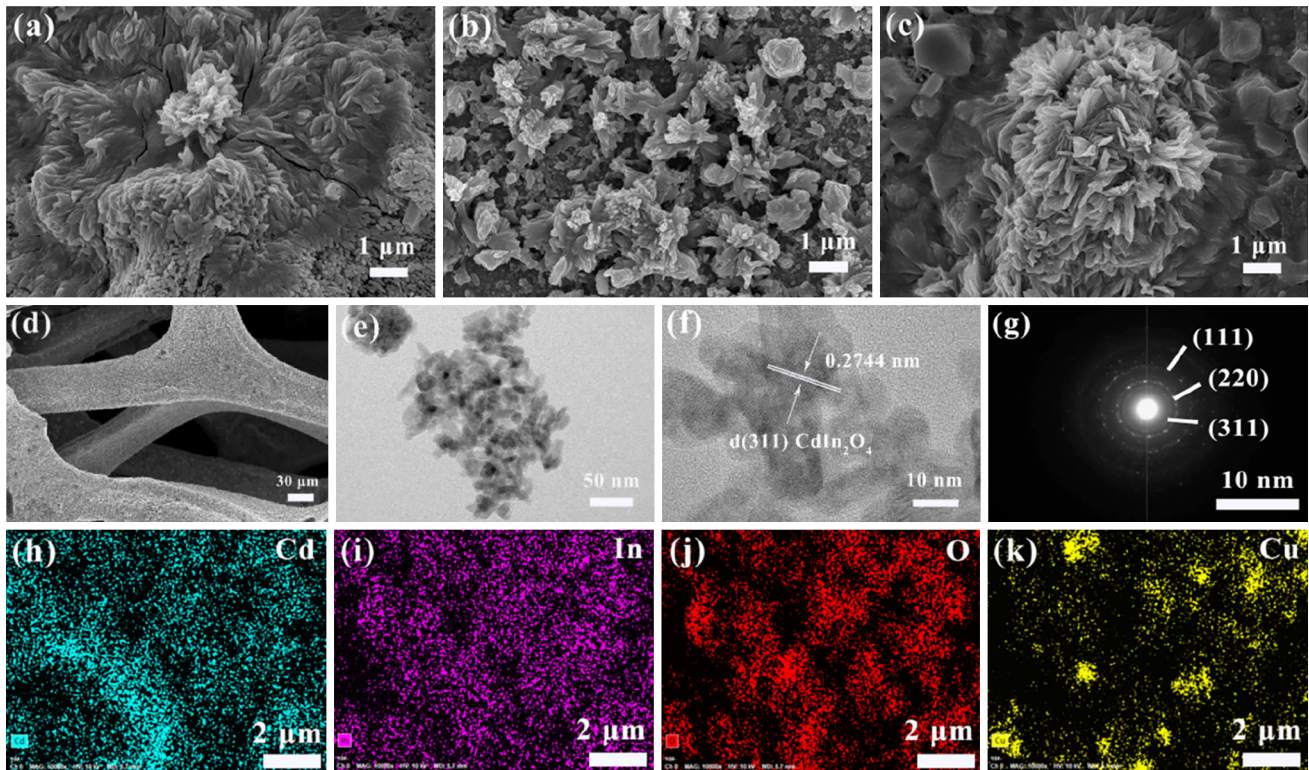


Fig. 3 SEM images: **a–c** 10%, 15%, and 20% Cu–CdIn₂O₄ decorated on Ni foams, respectively, **d** 15% Cu–CdIn₂O₄ decorated on Ni foam (low magnification). TEM image: **e** 15% Cu–CdIn₂O₄ nanoparticles. HRTEM image: **f** 15% Cu–CdIn₂O₄

nanoparticles. **g** SAED pattern of 15% Cu–CdIn₂O₄ nanoparticles. Elemental mapping of 15% Cu–CdIn₂O₄ nanoparticles for **h** Cd element, **i** In element, **j** O element, and **k** Cu elements

exhibits the space skeleton of 15% Cu–CdIn₂O₄ particles decorated on Ni foam, and the particles are tightly attached to the skeleton, which is beneficial to enhance the conductivity of the whole electrode. TEM image of 15% Cu–CdIn₂O₄ nanoparticles is shown in Fig. 3e, clearly displaying the dispersed particles. An HRTEM image (Fig. 3f) reveals the clear parallel fringes of (311) crystal planes of CdIn₂O₄ with a interplanar spacing value of 0.274 nm, which is shorter than the standard interplanar spacing value (0.277 nm) of pure CdIn₂O₄ phase, indicating that the Cu ions are successfully doped in CdIn₂O₄. Figure 3g presents a selected area of the electron diffracted pattern (SAED) with continuous rings, belonging to the (111), (220), and (311) planes of CdIn₂O₄. To further investigate the distribution of elements of 15% Cu–CdIn₂O₄ nanoparticles, EDS is also applied. The elemental mapping images (Fig. 3h–k) show that the 15% Cu–CdIn₂O₄ nanoparticles are composed of Cd, In, O, and Cu elements, and they are uniformly existed in the 15% Cu–CdIn₂O₄ nanoparticles.

XPS measurement is adopted to determine the chemical and surface state of the prepared nanocomposites. The survey spectra (Fig. 4a) of 10%, 15%, and 20% Cu–CdIn₂O₄ nanocomposites exhibit the peaks corresponding to the Cd, In, O, and Cu elements, respectively. Figure 4b shows the high-resolution scans of O 1s in all the prepared samples. The O 1s peak could be decomposed into two fitted peaks (oxygen vacancy and lattice oxygen are expressed as O_V and O_L, respectively). It is observed that the O_V peak of 15% Cu–CdIn₂O₄ sample shows the highest relative peak area, indicating it possesses more oxygen vacancy. The increase of O_V means that more adsorbed oxygen (O_x[−]) exists on the surface of the sample, and it can combine with H⁺ in the electrolyte to form O–H, which contributes to the hydrolysis of CdIn₂O₄ and promotes the redox reaction. Hence, 15% Cu–CdIn₂O₄ shows better electrochemical glucose detection in our following discussions. Figure 4c–e shows the high-resolution scans of Cd 3d, In 3d, and Cu 2p in 15% Cu–CdIn₂O₄, respectively. Two characteristic peaks at 404.84 eV

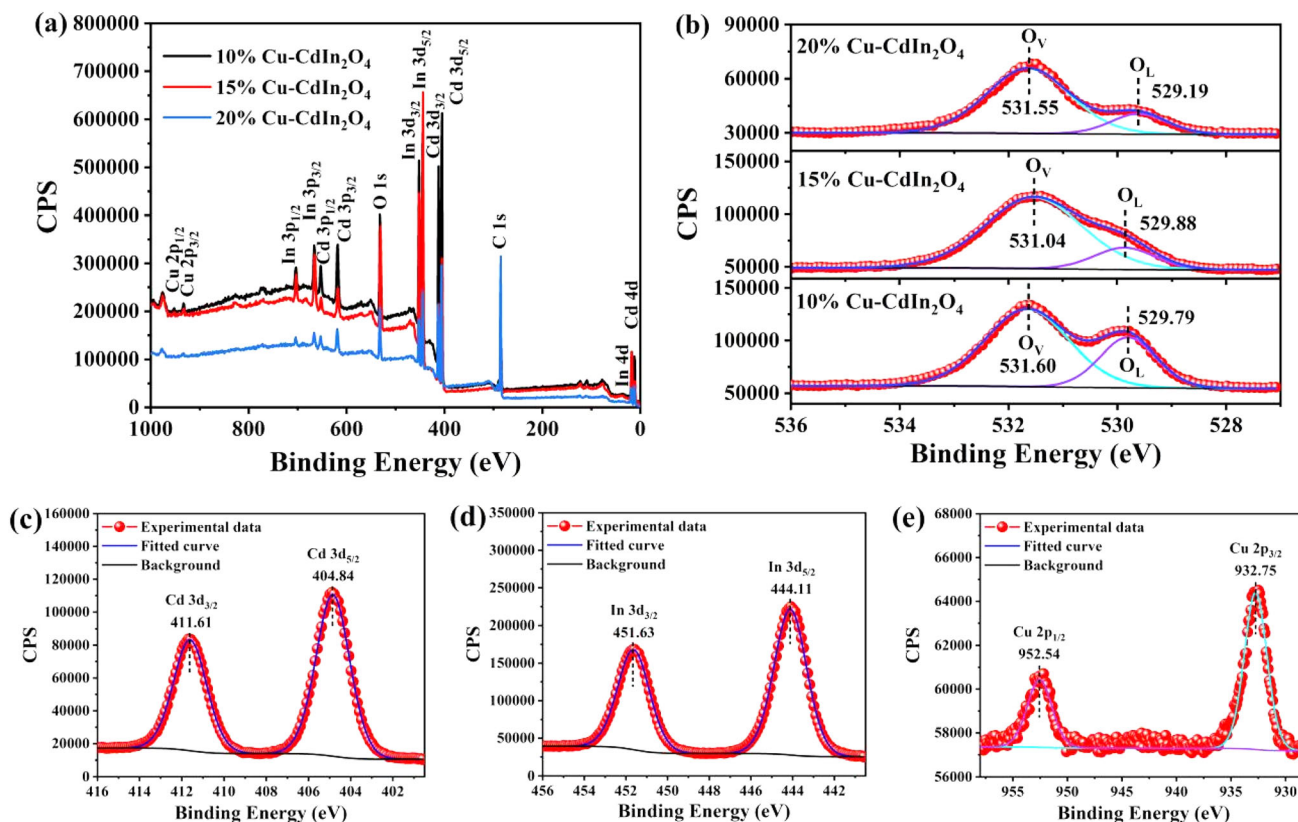


Fig. 4 XPS spectra of 15% Cu–CdIn₂O₄ nanoparticles. **a** Survey. High-resolution scans of **b** Cd 1s, **c** In 1s, **d** O 2p, **e** Cu 3d

and 411.61 eV are assigned to the Cd 3d_{5/2} and Cd 3d_{3/2} binding energies for Cd²⁺. The peaks at 444.11 eV and 451.63 eV are In 3d_{5/2} and In 3d_{3/2} of In 3d, which are attributed to lattice indium in CdIn₂O₄. The high-resolution scans of Cu 2p can be fitted as Cu 2p_{1/2} and Cu 2p_{3/2} peaks, and the binding energies of the two peaks are located at 952.54 eV and 932.75 eV, respectively.

3.2 Electrochemical performance of Cu–CdIn₂O₄ nanoparticles on Ni foams

The electrochemical impedance spectroscopy (EIS) behaviors of 10%, 15%, and 20% Cu–CdIn₂O₄/Ni foam electrodes are shown in Fig. 5. It can be observed that the semicircle diameter of the curve for 15% Cu–CdIn₂O₄/Ni foam electrode is smaller than that of 10% and 20% Cu–CdIn₂O₄/Ni foam electrodes at high frequency region, suggesting the fast charge-transfer rate and better electrical conductivity for 15% Cu–CdIn₂O₄/Ni foam electrode. Additionally, the intersection of the curves and the real axis is basically at the zero position, which indicates that there is a low internal resistance of the electrodes and better

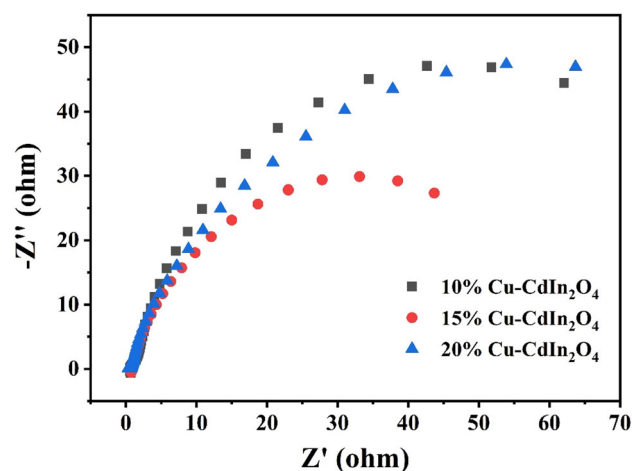


Fig. 5 Nyquist plots of EIS for the 10%, 15%, and 20% Cu–CdIn₂O₄ nanoparticles/Ni foam electrodes

electrical conductivity for the prepared Cu–CdIn₂O₄ nanoparticles.

The CV curves of the prepared 10%, 15%, 20% Cu–CdIn₂O₄ nanoparticles on Ni foams and bare Ni foam electrodes in 200 mL 3.5 M KOH electrolyte solution with and without 1 mM glucose are shown in Fig. 6a.

The current density of the 10%, 15%, 20% Cu–CdIn₂O₄ nanoparticles on Ni foams and bare Ni foam electrodes increases in the presence of glucose, indicating the glucose catalytic activity. The current density of bare Ni foam and CdIn₂O₄ nanoparticles on Ni foam electrodes in our previous work [32] is much lower than that of the Cu–CdIn₂O₄ electrodes, which indicates that doping a certain amount of Cu in CdIn₂O₄ nanoparticles on Ni foam would efficiently enhance the electrocatalytic activity. Meanwhile, the current response in 15% Cu–CdIn₂O₄ /Ni foam electrode is higher than that of 10% and 20% Cu–CdIn₂O₄/Ni foams electrodes, and the order can be expressed as 15% > 20% > 10%, suggesting that the 15% Cu–CdIn₂O₄/Ni foam electrode performs the best glucose-sensitive electrochemistry behavior. To further obtain the electrochemical kinetic information of electrocatalytic oxidation of glucose, the effect of scan rate on glucose oxidation at 15% Cu–CdIn₂O₄/Ni foam electrode is investigated in 3.5 M KOH electrolyte solution containing 1 mM glucose. As shown in Fig. 6b, the anodic peak-to-cathodic peak potential separation in the CV responses increases with the increase in the scan rate, which is attributed to the transport barriers of electrons and electrolyte ions during electrochemical processes, indicating the charge-transfer kinetic limitations [33]. Meanwhile, Fig. 6c shows the linearity between both the anodic peak current density (I_{pa}) and cathodic peak current density (I_{pc}) and the square root of the scan rate in the range from 10 to 180 mV s⁻¹, and the linear equation is as follows. The linear relationship indicates that the electrochemical process is dominated by the diffusion-controlled process [34, 35].

$$I_{pa} = 11.925v^{1/2} - 19.7164 \tag{1}$$

$$I_{pc} = -9.466v^{1/2} + 26.7642 \tag{2}$$

Simultaneously, the diffusion coefficient ratio between 15% Cu–CdIn₂O₄/Ni foam electrode and pristine CdIn₂O₄/Ni foam electrode [32] can be obtained by using Randles–Sevcik formula [36]:

$$D_{Cu-Cd}/D_{Cd} = \left[\frac{(I_{pa}/v^{1/2})_{Cu-Cd}}{(I_{pa}/v^{1/2})_{Cd}} \right]^2 \tag{3}$$

$$= (11.925/5.097)^2 = 5.47$$

The calculated result shows that the diffusion coefficient of 15% Cu–CdIn₂O₄/Ni foam electrode (D_{Cu-Cd}) is 5.47-fold that of pristine CdIn₂O₄ electrode (D_{Cd}), indicating that 15% Cu–CdIn₂O₄/Ni foam electrode displays better electrochemical performance than pristine CdIn₂O₄.

The amperometric sensing responses of 10%, 15%, and 20% Cu–CdIn₂O₄/Ni foam electrodes are investigated towards different concentration of glucose from 0.001 to 1 mM ($R^2 = 0.99$) at a constant voltage of 0.45 V, and the glucose solution is added every 50 s in a continuously stirred 3.5 M KOH electrolyte solution. As shown in Fig. 7a, c, and e, the current response exhibits a linear stable stepwise rise with the increase of glucose concentration. However, the curves deviate from linearity in the low concentration glucose range, which may be due to the instability of the initial current of the electrodes. The sensitivity is obtained by observing the corresponding slope parameter, as shown in Fig. 7b and d, the sensitivity of 10% and 15% Cu–CdIn₂O₄/Ni foam electrodes is 3.810 and 5.360 mA mM⁻¹ cm⁻² in 0.01–1.0 glucose

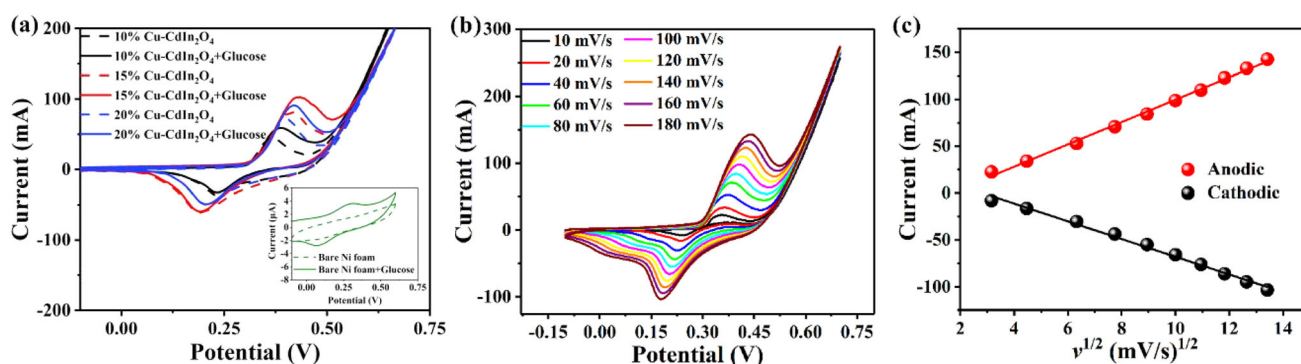


Fig. 6 a CV curves of Cu–CdIn₂O₄ nanoparticles/Ni foam electrodes in 3.5 M KOH electrolyte solution at a scan rate of 50 mV s⁻¹ with and without 1 mM glucose; b CV curves of 15%

Cu–CdIn₂O₄ nanoparticles/Ni foam electrode at different scan rates. c Linear plots of peak current density versus the square root of the scan rate

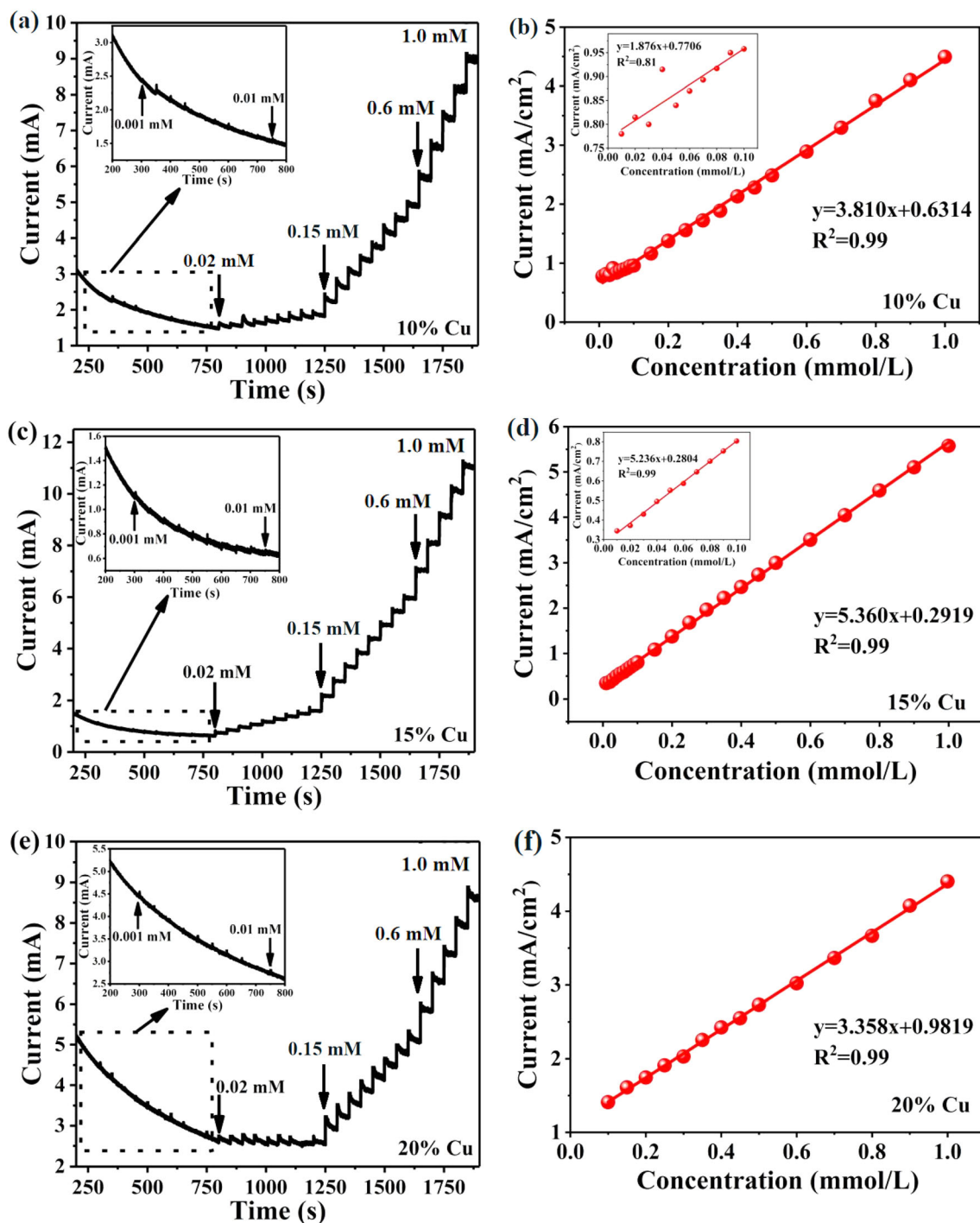


Fig. 7 The amperometric *I-t* curves of **a** 10% Cu-CdIn₂O₄ nanoparticles/Ni foam electrode, **c** 15% Cu-CdIn₂O₄ nanoparticles/Ni foam electrode, **e** 20% Cu-CdIn₂O₄ nanoparticles/Ni foam electrode upon the addition of various concentration of glucose at 0.45 V. Corresponding calibration

concentration range, respectively. The sensitivity of 20% Cu-CdIn₂O₄/Ni foam electrode in Fig. 7f shows 3.358 mA mM⁻¹ cm⁻² in the 0.1–1.0 glucose

concentration range, respectively. The 15% Cu-CdIn₂O₄/Ni foam electrode performs the highest electrochemical sensing response towards glucose detection compared

concentration range. The 15% Cu-CdIn₂O₄/Ni foam electrode performs the highest electrochemical sensing response towards glucose detection compared

with the other two electrodes, implying the excellent electrochemical catalytic oxidation reaction at the surface of 15% Cu–CdIn₂O₄ nanoparticles. However, the low response of 20% Cu–CdIn₂O₄/Ni foam electrode to glucose may be due to the inactivity of the second phase substance for glucose detection. Detection limit of the electrodes for glucose can be calculated by the formula $LOD = 3\sigma/S$, where σ is the standard deviation of the intercept and S is the slope of the calibration plot. The detection limit of 10%, 15%, and 20% Cu–CdIn₂O₄/Ni foam electrodes is 3.42, 3.39, and 4.11 μ M, respectively. In addition, a comparison of various non-enzymatic glucose sensors in previous works is shown in Table 1. Obviously, 15% Cu–CdIn₂O₄/Ni foam electrode in our work displays a higher sensitivity towards glucose detection. It may benefit from the synergistic interactions between Cu(II)/Cu(III) and Cd(II)/Cd(III), In(II)/In(III).

Figure 8a shows the enlarged section of the $I-t$ curve of 15% Cu–CdIn₂O₄/Ni foam electrode at 0.02 mM glucose concentration region, which tells that the current response increases sharply and reaches a steady state within 4 s, indicating a short response time of the proposed non-enzymatic glucose sensor. Anti-interference property is an important aspect of evaluating glucose sensor performance in practical applications. Figure 8b illustrates the anti-interference property of 15% Cu–CdIn₂O₄/Ni foam electrode by successive injection of 50 μ M glucose, 5 μ M ascorbic acid (AA), 5 μ M sodium chloride (NaCl), 5 μ M sodium nitrate (NaNO₃), 5 μ M Urea, and 5 μ M potassium chloride (KCl) at an interval of 50 s into 3.5 M KOH electrolyte solution under

continuous stirring. The result indicates that there is a high response to glucose, on the contrary, it is difficult to observe an obvious current response to AA, NaCl, NaNO₃, and KCl. Then, we continue to test the current response of all the interference species again, it can be observed that the electrode still shows the same response as the first cycle, suggesting its superior anti-interference property and excellent reproducibility, which can be reused continuously.

The long-term stability is also an important parameter for assessing sensor reliability in the practical application. Figure 9 displays the current signal and glucose sensitivity of 15% Cu–CdIn₂O₄/Ni foam electrode within 10 days in 3.5 M KOH electrolyte solution. It is observed that the current response values of the electrode still be maintained at more than 90% on day 10 compared with the initial value due to the electrode aging and the disappearance of unstable adsorption sites, suggesting its better electrocatalytic activity and satisfactory stability.

In order to verify the applicability of the 15% Cu–CdIn₂O₄/Ni foam glucose sensor, the glucose concentration is detected using the current–time method by successive step addition of the glucose to 200 mL stirred 3.5 M KOH electrolyte solution containing human serum samples. The test is executed three times, and the results are shown in Table 2. The recoveries of the 15% Cu–CdIn₂O₄/Ni foam non-enzymatic glucose sensor display in the range of 96.00–103.16% and the RSD is 2.11–3.56%, illustrating the potential use of as-synthesized Cu–CdIn₂O₄/Ni foam non-enzymatic glucose sensor in real serum sample analysis.

Table 1 A comparison of the non-enzymatic glucose sensors with various published materials

Materials	Sensitivity (μ A·mM ⁻¹ ·cm ⁻²)	Linear range (mM)	Detection limit (μ M)	References
Co ₃ O ₄ nanoclusters	1377	0.088–7	26	[37]
Ni(OH) ₂ flakes	2617	0.0025–1.050	2.5	[38]
Au-NPs/ZnO-NRs	157.34	0.5–10	55	[39]
NiCo ₂ O ₄ /ECF	1947.2	0.005–19.18	1.5	[40]
NiMn-LDH/GO	839.2	0.002–3.386	1.2	[41]
Cu/CuO/Cu(OH) ₂	223.17	0–20	20	[42]
CuO/Cu ₂ O film	1950	0.1–6	1	[43]
Cu ₂ O nanocubes	1040	0.007–4.5	3.1	[44]
CdIn ₂ O ₄	3292.5	0.001–1.0	0.08	[32]
Cu–CdIn ₂ O ₄	5360	0.01–1.0	3.39	This work

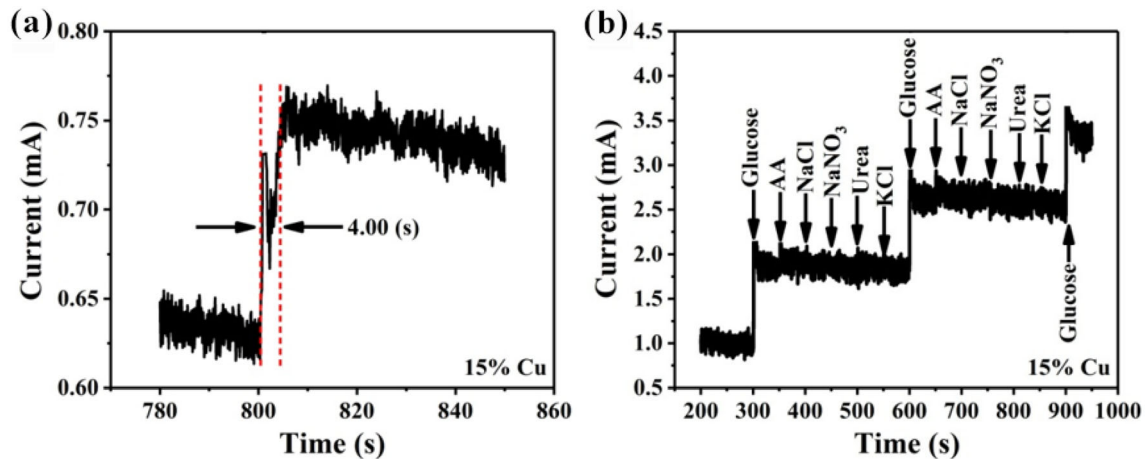


Fig. 8 **a** Response time of the enlarged section of the I–t curve of 15% Cu–CdIn₂O₄/Ni foam electrode at 0.02 mM glucose concentration region. **b** Amperometric response of the 15% Cu–CdIn₂O₄/Ni foam electrode with successive additions of different analytes

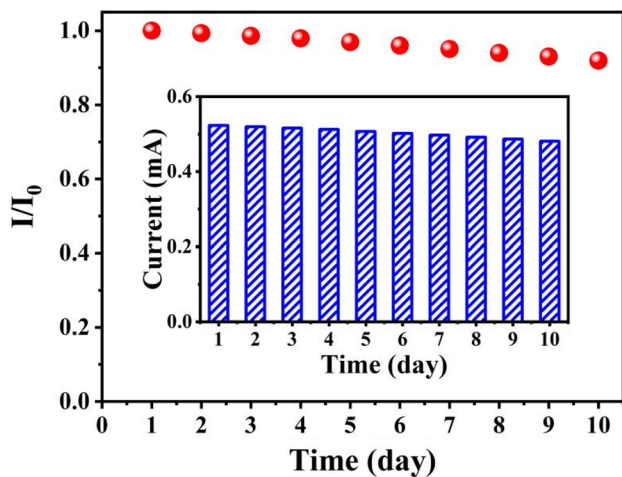


Fig. 9 Long-term stability of 15% Cu–CdIn₂O₄ nanoparticles/Ni foam electrode within 10 days

3.3 Glucose-sensing mechanism

The above-mentioned experimental results confirm that the 15% Cu–CdIn₂O₄/Ni foam electrode has apparent improvement in glucose sensitivity and its reliable utility in the detection of serum glucose in humans. As shown in Fig. 6a, b, there are obvious redox couple under alkaline conditions, which means

that Cd(II)/Cd(III) and In(II)/In(III) complete the current response to glucose, and Cu(II)/Cu(III) also participates in the catalytic process, making it more responsive to glucose than pristine CdIn₂O₄. Combining Fig. 10, a surface depletion layer model caused by glucose is used to illustrate the proposed mechanism for the sensing behavior of Cu–CdIn₂O₄/Ni foam electrode. When the electrode in the KOH electrolyte solution, the Cd(II), In(II), and Cu(II) are oxidized to Cd(III), In(III), and Cu(III) in electrolyte, simultaneously, electrons are taken away from the conduction band of the Cu–CdIn₂O₄ and the potential barrier increase, which results in a low conductivity. When glucose is added to the electrolyte, Cd(III), In(III), and Cu(III) catalyze the glucose to gluconolactone, while Cd(III), In(III), and Cu(III) are reduced to Cd(II), In(II), and Cu(II), in turn, electrons are released come back to conduction band and increase the oxidation peak current. The detail catalytic oxidation reactions towards glucose can be described as follows:

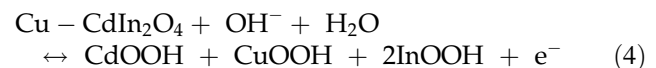


Table 2 Analysis of glucose in human serum samples on 15% Cu–CdIn₂O₄/Ni foam electrode

Samples	Glucose added (mmol/L)	Glucose found (mmol/L)	Recovery (%)	RSD (%) (n = 3)
1	0.2	0.192	96.00	2.11
2	0.4	0.405	101.25	2.79
3	0.6	0.619	103.16	3.56

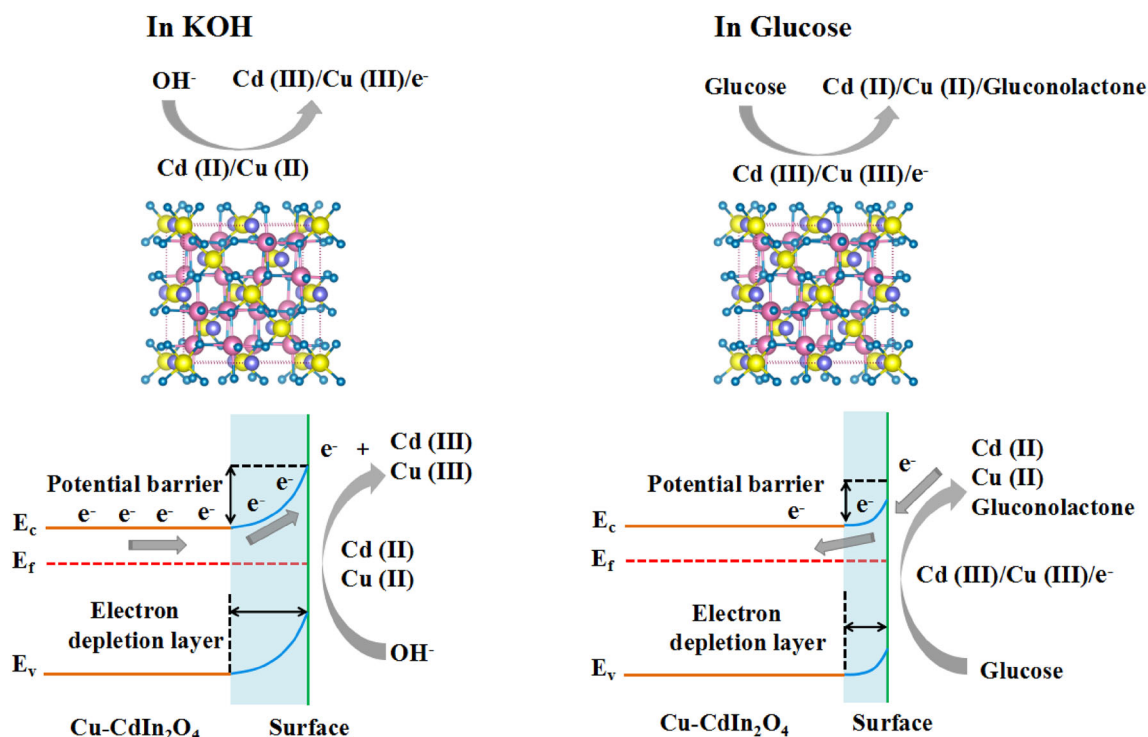
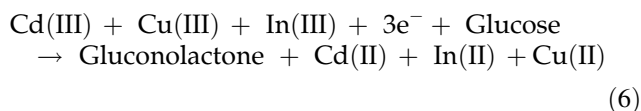
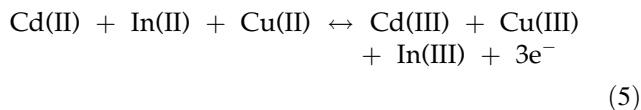


Fig. 10 Schematic illustration of the proposed gas-sensing mechanism and the energy band diagrams of electrode towards glucose detection



4 Conclusion

In this work, 10%, 15%, and 20% Cu-doped CdIn_2O_4 nanoparticles decorated on nickel foams as the sensitive non-enzymatic electrochemical sensors are successfully synthesized via a one-step non-aqueous sol-gel method and their electrochemical performance and glucose-sensing properties are investigated. The crystal phase, morphology, and chemical composition of the nanoparticles are systematically characterized by XRD, SEM, TEM, and XPS techniques, respectively. The results of the glucose-sensitive electrochemistry behavior of $\text{Cu-CdIn}_2\text{O}_4/\text{Ni}$ foam electrode indicate that Cd, In, and Cu jointly promote the electrochemical catalytic reaction in a

three-electrode system (3.5 KOH as electrolyte) to achieve a highly sensitive response to glucose. Additionally, the doping content of Cu also has a great influence on the performance, among which 15% $\text{Cu-CdIn}_2\text{O}_4/\text{Ni}$ foam electrode shows the best electrochemical performance towards glucose detection compared with 10% and 20% $\text{Cu-CdIn}_2\text{O}_4/\text{Ni}$ foam electrodes, such as higher sensitivity ($5303 \mu\text{A}\cdot\text{mM}^{-1}\cdot\text{cm}^{-2}$), faster response time (4 s), and wide linear range (0.1–1 mM), along with remarkable selectivity, long-term stability, which could be used as an efficient and sensitive glucose monitor in the practical workplace. Such satisfactory performance of 15% $\text{Cu-CdIn}_2\text{O}_4$ sample is not only attributed to the more oxygen vacancy, the smaller particle size which possesses higher specific surface area and reactive sites compared with 10% and 20% $\text{Cu-CdIn}_2\text{O}_4$, but also benefits from the synergistic effect of Cd, In, and Cu for the electrochemical catalytic reaction.

Acknowledgements

This work was supported by the National Natural Science Foundation of China (No. 61761047 and

41876055), the Yunnan Provincial Department of Science and Technology through the Key Project for the Science and Technology (Grant No.2017FA025), Program for Innovative Research Team (in Science and Technology) in University of Yunnan Province, and Project of the Department of Education of Yunnan Province (2022Y003).

Author contributions

All authors contributed to the work conception and design. Investigation, material preparation, and original draft writing were performed by XT and SP. Data curation, methodology, and analysis were performed by HS, TL, and ZY. TC, XX, and YW performed the supervision, writing—review and editing. All authors read and approved the final manuscript.

Data availability

This work described has not been published before. All data generated or analyzed during this study are included in this published article.

Declarations

Conflict of interest The authors have no relevant financial or non-financial interests to disclose.

Ethical approval The work contains no libelous or unlawful statements, does not infringe on the rights of others, or contains material or instructions that might cause harm or injury.

References

- S. Yu, L. Ding, H. Lin, W. Wu, J. Huang, A novel optical fiber glucose biosensor based on carbon quantum dots-glucose oxidase/cellulose acetate complex sensitive film. *Biosensors Bioelectron.* **146**, 111760 (2019)
- V. Rachim, W. Chung, Wearable-band type visible-near infrared optical biosensor for non-invasive blood glucose monitoring. *Sensors Actuators B Chem.* **286**, 173–180 (2019)
- J. Luo, P. Luo, M. Xie, K. Xie, B. Zhao, F. Pan, F. Zeng, D. Zhang, Z. Zheng, A new type of glucose biosensor based on surface acoustic wave resonator using Mn-doped ZnO multilayer structure. *Biosensors Bioelectron.* **49**, 512–518 (2013)
- D. Hwang, S. Lee, M. Seo, T. Chung, Recent advances in electrochemical non-enzymatic glucose sensors—a review. *Anal. Chim. Acta* **1033**, 1–34 (2018)
- B. Huang, Y. Wang, Z. Lu, H. Du, J. Ye, One pot synthesis of palladium cobalt nanoparticles over carbon nanotubes as a sensitive non-enzymatic sensor for glucose and hydrogen peroxide detection. *Sensors Actuators B Chem.* **252**, 1016–1025 (2017)
- N. Karikalan, M. Velmurugan, S. Chen, C. Karuppiah, Modern approach to the synthesis of Ni(OH)₂ decorated sulfur doped carbon nanoparticles for the nonenzymatic glucose sensor. *ACS Appl. Mater. Interfaces* **8**, 22545–22553 (2016)
- S. Zaidi, J. Shin, Recent developments in nanostructure based electrochemical glucose sensors. *Talanta* **149**, 30–42 (2016)
- J. Li, H. Hu, H. Li, C. Yao, Recent developments in electrochemical sensors based on nanomaterials for determining glucose and its by product H₂O₂. *J. Mater. Sci.* **52**, 10455–10469 (2017)
- H. Zhu, L. Li, W. Zhou, Z. Shao, X. Chen, Advances in non-enzymatic glucose sensors based on metal oxides. *J. Mater. Chem. B.* **4**, 7333–7349 (2016)
- B. Huang, M. Wang, D. Kathiravan, A. Kurniawan, H. Zhang, W. Yang, Interfacial effect of oxygen-doped nanodiamond on CuO and micro-pyramidal silicon heterostructures for efficient non-enzymatic glucose sensor. *ACS Appl. Bio Mater.* **1**, 1579–1586 (2018)
- J. Chen, H. Yin, J. Zhou, J. Gong, L. Wang, Y. Zheng, Q. Nie, Non-enzymatic glucose sensor based on nickel nitride decorated nitrogen doped carbon spheres (Ni₃N/NCS) via facile one pot nitridation process. *J. Alloys Compd.* **797**, 922–930 (2019)
- T. Liu, M. Li, P. Dong, Y. Zhang, L. Guo, Design and facile synthesis of mesoporous cobalt nitride nanosheets modified by pyrolytic carbon for the nonenzymatic glucose detection. *Sens. Actuator B Chem.* **255**, 1983–1994 (2018)
- F. Xie, X. Cao, F. Qu, A.M. Asiri, X. Sun, Cobalt nitride nanowire array as an efficient electrochemical sensor for glucose and H₂O₂ detection. *Sensors Actuators B Chem.* **255**, 1254–1261 (2018)
- Y. Ding, Y. Wang, L. Su, M. Bellagamba, H. Zhang, Y. Lei, Electrospun Co₃O₄ nanofibers for sensitive and selective glucose detection. *Biosensors Bioelectron.* **26**, 542–548 (2010)
- Q. Dong, D. Song, Y. Huang, Z. Xu, J. Chapman, W. Willis, B. Li, Y. Lei, High-temperature annealing enabled iridium oxide nanofibers for both non-enzymatic glucose and solid-state pH sensing. *Electrochim. Acta* **281**, 117–126 (2018)

16. J. Xu, Y. Sun, J. Zhang, Solvothermal synthesis of Fe_3O_4 nanospheres for high-performance electrochemical non-enzymatic glucose sensor. *Sci. Rep.* **10**, 16026 (2020)
17. J. Zhang, C. Xu, R. Zhang, X. Guo, J. Wang, X. Zhang, D. Zhang, B. Yuan, Solvothermal synthesis of cobalt tungstate microrings for enhanced nonenzymatic glucose sensor. *Mater. Lett.* **210**, 291–294 (2018)
18. W. Wu, L. Wu, H. Wu, S. Wang, Y. Ding, C. Feng, Sulphides of the cobalt doped Ni_7S_6 type for glucose, hydrogen peroxide and nitrite sensing platform. *Sensors Actuators B Chem.* **250**, 224–232 (2017)
19. C. Zhao, X. Wu, X. Zhang, P. Li, X. Qian, Facile synthesis of layered CuS/RGO/CuS nanocomposite on Cu foam for ultrasensitive nonenzymatic detection of glucose. *J. Electroanal. Chem.* **785**, 172–179 (2017)
20. V. Sridhar, H. Park, Carbon encapsulated cobalt sulfide nanoparticles anchored on reduced graphene oxide as high capacity anodes for sodium-ion batteries and glucose sensor. *J. Alloys Compd.* **764**, 490–497 (2018)
21. P. Liu, M. Zhang, S. Xie, S. Wang, W. Cheng, F. Cheng, Non-enzymatic glucose biosensor based on palladium-copper oxide nanocomposites synthesized via galvanic replacement reaction. *Sensors Actuators B Chem.* **253**, 552–558 (2017)
22. C. Wang, Y. Sun, X. Yu, D. Ma, J. Zheng, P. Dou, Z. Cao, X. Xu, Ag–Pt hollow nanoparticles anchored reduced graphene oxide composites for non-enzymatic glucose biosensor. *J. Mater. Sci. Mater. Electron.* **27**, 9370–9378 (2016)
23. C. Xia, W. Ning, A novel non-enzymatic electrochemical glucose sensor modified with FeOOH nanowire. *Electrochem. Commun.* **12**, 1581–1584 (2010)
24. R. Ding, L. Qi, M. Jia, H. Wang, Facile synthesis of mesoporous spinel NiCo_2O_4 nanostructures as highly efficient electrocatalysts for urea electro-oxidation. *Nanoscale* **6**, 1369–1376 (2014)
25. Y. Zhang, L. Luo, Z. Zhang, Y. Ding, S. Liu, D. Deng, H. Zhao, Y. Chen, Synthesis of MnCo_2O_4 nanofibers by electrospinning and calcination: application for a highly sensitive non-enzymatic glucose sensor. *J. Mater. Chem. B.* **2**, 529–535 (2014)
26. H. Yin, Y. Shi, Y. Dong, X. Chu, Synthesis of spinel-type CuGa_2O_4 nanoparticles as a sensitive non-enzymatic electrochemical sensor for hydrogen peroxide and glucose detection. *J. Electroanal. Chem.* **885**, 115110 (2021)
27. X. Luo, M. Huang, D. He, M. Wang, Y. Zhang, P. Jiang, Porous NiCo_2O_4 nanoarray-integrated binder-free 3D open electrode offers a highly efficient sensing platform for enzyme-free glucose detection. *Analyst* **143**, 2546–2554 (2018)
28. S. Cui, S. Gu, Y. Ding, J. Zhang, Z. Zhang, Z. Hu, Hollow mesoporous CuCo_2O_4 microspheres derived from metal organic framework: a novel functional materials for simultaneous H_2O_2 biosensing and glucose biofuel cell. *Talanta* **178**, 788–795 (2018)
29. E. Kim, M. Imran, M. Akhtar, H. Shin, S. Ameen, Enticing 3D peony-like ZnGa_2O_4 microstructures for electrochemical detection of N,N-dimethylmethanamide chemical. *J. Hazard. Mater.* **404**, 124069 (2021)
30. Y. Liu, C. Kong, X. Lu, F. Liao, F. Huang, J. Lin, One-step hydrothermal synthesis of high-performance gas-sensing crystals CdIn_2O_4 with octahedral shape. *Cryst. Growth. Des.* **12**, 4104–4108 (2012)
31. D. Wang, D. Cai, H. Huang, B. Liu, L. Wang, Y. Liu, H. Li, Y. Wang, Q. Li, T. Wang, Non-enzymatic electrochemical glucose sensor based on NiMoO_4 nanorods. *Nanotechnology* **26**, 145501 (2015)
32. S. Peng, T. Lai, Y. Kong, Y. Ran, L. Su, D. Ma, X. Xiao, Y. Wang, A novel non-enzymatic glucose electrochemical sensor with high sensitivity and selectivity based on CdIn_2O_4 nanoparticles on 3D Ni foam substrate. *Nanotechnology* **32**, 405502 (2021)
33. B. Rafiee, A. Fakhari, Electrocatalytic oxidation and determination of insulin at nickel oxide nanoparticles-multiwalled carbonnanotube modified screen printed electrode. *Biosensors Bioelectron.* **46**, 130–135 (2013)
34. Y. Mu, D. Jia, Y. He, Y. Miao, H. Wu, Nano nickel oxide modified non-enzymatic glucose sensors with enhanced sensitivity through an electrochemical process strategy at high potential. *Biosens. Bioelectron.* **26**, 2948–2952 (2011)
35. J. Nai, S. Wang, Y. Bai, L. Guo, Amorphous $\text{Ni}(\text{OH})_2$ nanoboxes: fast fabrication and enhanced sensing for glucose. *Small* **9**, 3147–3152 (2013)
36. S. Liu, K. Hui, K. Hui, 1D hierarchical MnCO_2O_4 nanowire@ MnO_2 sheet core-shell arrays on graphite paper as superior electrode for asymmetric supercapacitors. *Chemnanomat.* **8**, 593–602 (2016)
37. L. Wang, Y. Zhang, Y. Xie, J. Yu, H. Yang, L. Miao, Y. Song, Three-dimensional macroporous carbon/hierarchical Co_3O_4 nanoclusters for nonenzymatic electrochemical glucose sensor. *Appl. Surf. Sci.* **402**, 47–52 (2017)
38. K. Xia, C. Yang, Y. Chen, L. Tian, Y. Su, J. Wang, L. Li, In situ fabrication of $\text{Ni}(\text{OH})_2$ flakes on Ni foam through electrochemical corrosion as high sensitive and stable binder-free electrode for glucose sensing. *Sensors Actuators B Chem.* **240**, 979–987 (2017)
39. P. Rattanawarinchai, N. Khemasiri, N. Soyeux, S. Jessadaluk, A. Klamchuen, S. Wirunchit, A. Rangkasikorn, N. Kayunkid, D. Phromyothin, S. Rahong, J. Nukeaw, Gold nanoparticles decorated zinc oxide nanorods as electrodes for a highly sensitive non-enzymatic electrochemical glucose detection. *J. Appl. Phys.* **58**, SDDE04 (2019)

40. L. Liu, Z. Wang, J. Yang, G. Liu, J. Li, L. Guo, S. Chen, Q. Guo, NiCo₂O₄ nanoneedle-decorated electrospun carbon nanofiber nanohybrids for sensitive non-enzymatic glucose sensors. *Sensors Actuators B Chem.* **258**, 920–928 (2018)
41. J. Zhou, M. Min, Y. Liu, J. Tang, W. Tang, Layered assembly of NiMn-layered double hydroxide on graphene oxide for enhanced non-enzymatic sugars and hydrogen peroxide detection. *Sensors Actuators B Chem.* **260**, 408–417 (2018)
42. P. Viswanathan, J. Park, D. Kang, J. Hong, Polydopamine-wrapped Cu/Cu(II) Nano-heterostructures: an efficient electrocatalyst for non-enzymatic glucose detection. *Colloids Surf. A* **580**, 123689 (2019)
43. R. Li, X. Liu, H. Wang, Y. Wu, K.C. Chan, Z. Lu, Sandwich nanoporous framework decorated with vertical CuO nanowire arrays for electrochemical glucose sensing. *Electrochim. Acta.* **299**, 470–478 (2019)
44. C. Espro, S. Marini, D. Giusi, C. Ampelli, G. Neri, Non-enzymatic screen printed sensor based on Cu₂O nanocubes for glucose determination in bio-fermentation processes. *J. Electroanal. Chem.* **873**, 114354 (2020)

Publisher's Note Springer Nature remains neutral with regard to jurisdictional claims in published maps and institutional affiliations.

Springer Nature or its licensor holds exclusive rights to this article under a publishing agreement with the author(s) or other rightsholder(s); author self-archiving of the accepted manuscript version of this article is solely governed by the terms of such publishing agreement and applicable law.